



## Eco-hydrological effects of stream-aquifer water interaction: A case study of the Heihe River Basin, northwestern China

Yujin Zeng<sup>1,2</sup>, Zhenghui Xie<sup>1</sup>, Yan Yu<sup>3</sup>, Shuang Liu<sup>1,2</sup>, Linying Wang<sup>1,2</sup>, Binghao Jia<sup>1</sup>, Peihua Qin<sup>1</sup>, Yaning Chen<sup>4</sup>

5

<sup>1</sup>State Key Laboratory of Numerical Modeling for Atmospheric Sciences and Geophysical Fluid Dynamics, Institute of Atmospheric Physics, Chinese Academy of Sciences, Beijing, 100029, China

<sup>2</sup>College of Earth Science, University of Chinese Academy of Sciences, Beijing 100049, China

<sup>3</sup>Zhejiang Institute of Meteorological Sciences, Hangzhou, 310008, China

10 <sup>4</sup>Key Laboratory of Oasis Ecology and Desert Environment, Xinjiang Institute of Ecology and Geography, Chinese Academy of Sciences, Urumqi, 830011, China

*Correspondence to:* Zhenghui Xie ([zxie@lasg.iap.ac.cn](mailto:zxie@lasg.iap.ac.cn))

15 **Abstract.** A scheme describing the process of stream-aquifer interaction was incorporated into the land model CLM4.5 to investigate the effects of stream water conveyance over riparian banks on ecological and hydrological processes. Two groups of simulations for five typical river cross-sections in the middle reaches of the arid zone Heihe River Basin were conducted. The simulated riparian groundwater table at a propagation distance of less than 1 km followed the intra-annual fluctuation of the river water level, and the correlation was excellent ( $R^2 = 0.9$ ) between the river water level and the groundwater table at  
20 the distance 60 m from the river. The correlation rapidly decreased as distance increased. In response to the variability of the water table, soil moisture at deep layers also followed the variation of river water level all year, while soil moisture at the surface layer was more sensitive to the river water level in the drought season than in the wet season. With increased soil moisture, the average gross primary productivity and respiration of riparian vegetation within 300 m from the river at a typical section of the river increased by approximately  $0.03 \text{ mg C m}^{-2} \text{ s}^{-1}$  and  $0.02 \text{ mg C m}^{-2} \text{ s}^{-1}$ , respectively, in the growing  
25 season. Consequently, the net ecosystem exchange increased by approximately  $0.01 \text{ mg C m}^{-2} \text{ s}^{-1}$ , and the evapotranspiration increased by approximately  $3 \text{ mm d}^{-1}$ . Furthermore, the length of the growing season of riparian vegetation also increased by 2–3 months due to the sustaining water recharge from the river.



## 1 Introduction

Water in streams and aquifers are closely related and both resources have important roles in the carbon-water cycle and in supplying human needs (Chen and Xie, 2010, 2012; Yu et al., 2014; Zou et al., 2014, 2015; Xie et al., 2014). In a wet region, rainfall or melting snow can raise the groundwater table to an elevation higher than that of the vicinal stream level; groundwater also sustains base flow in streams and rivers (Arnold et al., 2000). In an arid region, groundwater is recharged laterally from rivers to unconfined aquifers by the stream water conveyance, which sustains the terrestrial ecosystem along the natural channel (Scanlon et al., 2002; Chen et al., 2004, 2010) and induces an increase of riparian soil moisture, soil evaporation, and vegetation transpiration. The growth of riparian vegetation and subsequently changes in carbon cycle processes respond to the water supplement of streams. Understanding and quantifying the effects of stream water conveyance over riparian banks on ecological-hydrological processes is of significance for water resources management (Baskaran et al., 2009).

To investigate the interaction between groundwater and climate, Liang et al. (2003) and Liang and Xie (2003) presented a new parameterization to represent surface and groundwater dynamics and implemented it into the variable infiltration capacity model. Studies have documented that the interaction between surface water and groundwater significantly affect the partition of the water budget and then the land-atmosphere interaction (Maxwell et al., 2007; Maxwell and Kollet, 2008; Fan and Miguez-Macho, 2010, 2011; Fan et al., 2015). To predict the water table elevation near a river channel in an arid region from river discharge, Xie and Yuan (2010) developed a statistical-dynamical approach, whereas Di et al. (2011) and Xie et al. (2012) each developed a quasi two-dimension and quasi three-dimension variably saturated groundwater flow model. These works focused on the temporal and spatial variation of the groundwater table and soil moisture in a riverbank. However, the impacts of river-aquifer water exchange on ecological-hydrological processes, including energy and vapor fluxes, gross primary productivity (GPP) and net ecosystem exchange (NEE) for the riparian ecosystem are not fully represented in previous research. In this study, we incorporated a scheme for stream-aquifer water interaction into the Community Land Model Version 4.5 (CLM4.5), which contains descriptions about the energy, biophysical and biochemical processes of the land surface and sub-surface, to investigate the effects of stream-aquifer interaction over the Heihe River Basin, a typical region having an arid climate.



In Sect. 2 of this paper, the model development are specifically described, while some background information about the study domain and the experimental design are described in Sect. 3. Section 4 contains the results of simulations and the corresponding analysis. The conclusions and discussion are presented in Sect. 5.

## 2 Model development

### 5 2.1 Community Land Model4.5

The land surface model CLM4.5 was developed by the National Center for Atmospheric Research (Oleson et al., 2013), and is the land component of the Community Earth System Model 1.2.0 (Gent et al., 2011; Hurrell et al., 2013). The CLM4.5 model simulates the biogeophysical exchange of radiation, sensible and latent heat flux; momentum between the land and atmosphere as modified by vegetation and soil; heat transfer in soil and snow; and the hydrologic cycle including precipitation interception, infiltration, runoff, soil water, groundwater table depth and snow dynamics (Lindsay et al., 2014). Bio-geochemical cycles including processes of the carbon and nitrogen cycles, photosynthesis, vegetation phenology, decomposition, and fire disturbances are also presented in CLM4.5. Evapotranspiration simulated by CLM4.5 is partitioned into evaporation and transpiration regulated by stoma physiology and photosynthesis. Specifically, CLM4.5 is a one-dimensional model in which physical and chemical processes are considered only in the vertical direction (lateral transits of water and energy are not included yet). More information about CLM4.5 is contained in the Journal of Climate (<http://journals.ametsoc.org/page/CCSM4/CESM1>).

### 2.2 Scheme for stream-aquifer interaction and its implementation into CLM4.5

The stream-aquifer water interaction scheme developed by Di et al. (2011) was incorporated into CLM4.5 (and called CLM\_RIV). We first describe the new model briefly as follows. Based on Darcy's law and the Dupuit approximation (Bear, 1972), the lateral flow between a river and the neighboring groundwater can be expressed as:

$$R(x, t) = \frac{\partial Q}{\partial x} = \frac{\partial}{\partial x} \left( T(x, t) \frac{\partial h(x, t)}{\partial x} \right), x > 0, t \geq 0, \quad (1)$$

while the corresponding initial and boundary conditions are expressed as:

$$h(x, 0) = h_0(x), \quad (2)$$



$$h(0, t) = h_{river}(t), \quad (3)$$

where  $x$  (L) is the perpendicular distance from the point on a bank to the river channel,  $t$  (T) is time,  $R(x, t)$  (L/T) is the lateral groundwater recharge (or discharge) rate at point  $x$  and time  $t$ ,  $Q$  [L<sup>2</sup>/T] is the lateral flow discharge,  $T(x, t)$  (L<sup>2</sup>/T) is the lateral flow transmissivity,  $h(x, t)$  (L) is the groundwater table elevation,  $h_0(x)$  (L) is the initial groundwater table elevation and  $h_{river}(t)$  (L) is the river water level, as shown in Figures 1a and 1b. If the river water level is higher in elevation than its neighboring groundwater table (as shown in Figure 1a),  $R(x, t)$  is greater than zero and the local aquifer is recharged by the stream; otherwise, as shown in Figure 1b,  $R(x, t)$  is less than zero and the local aquifer discharges to the stream.

To incorporate the stream-aquifer interaction scheme into CLM4.5, the continuity Eq. (1) should be discretized over a model grid and each variable should be linked to CLM4.5. Applying the zero-flux boundary condition to the outermost grid of the simulation domain, the discrete formation of Eq. (1) can be written as:

$$\left\{ \begin{array}{l} R_{1,n} = \frac{\frac{T_{0,n} + T_{1,n}}{2} \times \frac{h_m - h_{1,n}}{\Delta x / 2} - \frac{T_{1,n} + T_{2,n}}{2} \times \frac{h_{1,n} - h_{2,n}}{\Delta x}}{\Delta x} \\ R_{i,n} = \frac{\frac{T_{i-1,n} + T_{i,n}}{2} \times \frac{h_{i-1,n} - h_{i,n}}{\Delta x} - \frac{T_{i,n} + T_{i+1,n}}{2} \times \frac{h_{i,n} - h_{i+1,n}}{\Delta x}}{\Delta x}, \quad 2 \leq i \leq m-1, \quad (4) \\ R_{m,n} = \frac{\frac{T_{m-1,n} + T_{m,n}}{2} \times \frac{h_{m-1,n} - h_{m,n}}{\Delta x}}{\Delta x} \end{array} \right.$$

where  $i$  is the number of the grid that is successively added with the increasing distance from grid to channel (Figure 1c),  $m$  is the farthest grid from the river channel in the model (i.e., the outermost grid of the simulation domain),  $n$  is the number of the time step,  $R_{i,n}$  (L/T) is the lateral groundwater recharge (or discharge) rate of grid  $i$  at the  $n$ th time step,  $T_{i,n}$  (L<sup>2</sup>/T) is the lateral flow transmissivity,  $h_{i,n}$  (L) is the groundwater table elevation,  $h_m$  (L) is the river water level (which is another boundary condition of the simulation and will be discussed in Sect. 3.2), and  $\Delta x$  (L) is the side length of each model grid.



The variables  $h_{i,n}$ ,  $T_{i,n}$  and  $R_{i,n}$  ( $i > 0$ ) in Eq. (4) are linked to CLM4.5 as follows. The water table elevation  $h_{i,n}$  is easily obtained by subtracting the groundwater table depth from the ground elevation as:

$$h = h_e - z_{wt}, \quad (5)$$

where  $h_e$  (L) and  $z_{wt}$  (L) are, respectively, the ground elevation and current groundwater table depth of the grid calculated by CLM4.5. To obtain the lateral flow transmissivity  $T_{i,n}$ , we considered two cases in the model. In case A, the groundwater table is within the soil layers of the model (i.e., water table depth is deeper than 3.8m) and the transmissivity can be expressed as:

$$T = T_1 + T_2, \quad (6)$$

$$T_1 = \sum_{j=1}^{10} K_j \Delta z_j, \quad (7)$$

$$T_2 = \int_0^{\infty} K(z') dz' = \int_0^{\infty} K_{10} e^{-\frac{z'}{f}} dz' = K_{10} f, \quad (8)$$

where  $j$  is the number of soil layer denoted by CLM4.5,  $K_j$  (L/T) and  $f$  (L) are, respectively, the lateral hydraulic conductivity of the  $j$ th soil layer and the e-folding length (which will be discussed later), and  $\Delta z_j$  (L) is the thickness of the  $j$ th soil layer. Based on Fan et al. (2007), we also applied an estimation of the lateral hydraulic conductivity at depth below the 10th soil layer in Eq. (8) as:

$$K(z') = K_{10} e^{-\frac{z'}{f}}, \quad (9)$$

where  $K_{10}$  (L/T) is the lateral hydraulic conductivity at the 10th soil layer,  $z'$  (L) is the relative depth to the bottom boundary of the 10th soil layer, and  $K(z')$  (L/T) is the lateral hydraulic conductivity at relative depth  $z'$ . In CLM4.5, only the vertical hydraulic conductivity is provided. So to obtain the lateral hydraulic conductivity  $K_j$  of each soil layer, we applied the assumption of Fan et al. (2007) such that the lateral conductivity is related to the vertical hydraulic conductivity and the content of clay for local soil as:

$$K_j = K_j' \times P_{clay}, \quad (10)$$



where  $K_j'$  (L/T) is the vertical hydraulic conductivity provided by CLM4.5 and  $P_{clay}$  is the percentage of clay in local soil, as provided by surface data of CLM4.5. The e-folding length  $f$  in Eq. (8) is a parameter representing the local sediment-bedrock profile, which is complex depending on tectonics, weathering and erosion-deposition processes. In this study, we simply implemented an estimation of Fan et al. (2007) to relate e-folding length to terrain slope as:

$$f = \begin{cases} \frac{20}{1+125\beta}, & \beta \leq 0.16 \\ 1, & \beta > 0.16 \end{cases}, \quad (11)$$

where  $\beta$  (radian) represents the terrain slope and can be obtained from the surface data of CLM4.5.

In case B, where the groundwater table is positioned below the 10th soil layer of CLM4.5, the  $T_{i,n}$  can be calculated as:

$$T = \int_{z_{wt} - z_{i10}}^{\infty} K(z') dz' = \int_{z_{wt} - z_{i10}}^{\infty} K_{10} e^{-\frac{z'}{f}} dz' = K_{10} f e^{-\frac{z_{i10} - z_{wt}}{f}}, \quad (12)$$

where  $z_{i10}$  (L) is the lower boundary depth of the 10th soil layer of CLM4.5. We also applied the parameterization of Eq. (9) in Eq. (12).

In Eq. (4),  $T_{0,n}$  (L<sup>2</sup>/T) is the flow transmissivity of the river with respect to groundwater-river exchange. Based on Xie and Yuan (2010), flow transmissivity can be expressed as:

$$T_0 = K_r w, \quad (13)$$

where  $w$  (L) is the river width obtained from measured data and  $K_r$  (L<sup>2</sup>/T) is the hydraulic conductivity at the river bed (which will be discussed in Sect. 3.2).

Finally, the lateral water recharge (or discharge) rate  $R_{i,n}$  in Eq. (4) is linked to CLM4.5 as follows:

$$\begin{cases} z_{wt\_new} = z_{wt\_ori} - \frac{R \times \Delta t}{s_y}, \\ W_{new} = W_{ori} + R \times \Delta t \end{cases}, \quad (14)$$

where  $\Delta t$  (T) is the time step of CLM4.5,  $s_y$  is the aquifer specific yield calculated by CLM4.5,  $z_{wt\_ori}$  (L) and  $z_{wt\_new}$  (L) are, respectively, the original simulated groundwater table depth by CLM4.5 and the updated value after considering the



later flow flux, and  $W_{ori}$  (L) and  $W_{new}$  (L) are, respectively, the original simulated aquifer water storage by CLM4.5 and the updated value after considering the lateral flow flux.

Equations (4) to (14) are incorporated in CLM4.5 to renew the values of groundwater table depth and aquifer water storage at every time step. Other hydrological and ecological variables will be in turn be modified by these changes as the model continues to operate.

### 3 Study domain and experimental design

#### 3.1 Study domain

The Heihe River Basin is the second largest inland river basin in an arid area in Northern China. It is located between 96°42'E and 102°00'E and between 37°41'N and 42°42'N (Lu et al., 2003) (Figure 2). The basin covers 116,000 km<sup>2</sup> and lies to the east of the Shule River Basin and west of the Shiyang River Basin (Chen et al., 2005). In the upper reaches of the basin with obvious vertical zonal divisions, the mean annual precipitation is approximately 200 mm at elevations from 2000 m to 3200 m, and about 500 mm at elevations between 3200 m and 5500 m. The upper reaches are the main water resource of the entire basin (Wu et al., 2010). In the middle reaches, the elevation decreases from 2000 m to 1000 m and the precipitation correspondingly decreases from 200 mm to less than 100 mm in the direction from south to north (Li et al., 2001). The lower reaches, whose mean altitude is approximately 1000 m, is an arid region with a mean annual precipitation of only 42 mm according to statistics from meteorological stations (Qi and Luo, 2005).

In this study, five typical river cross-sections were chosen as test sites to simulate using our CLM\_RIV model. These sites were named, respectively, 213 Bridge, 312 Bridge, Tielu Bridge, Pingchuan Bridge and Gaotai Bridge, and all are located on the middle reaches of the Heihe River Basin. Among these sites, the 213 Bridge section was chosen to test the model's sensitivity, but all the five cross-sections were used in the actual model runs. The locations of these sections and relevant information about them are shown in Figure 3 and Table 1, respectively.

#### 3.2 Experimental design

Some ideal experiments to test the model sensitivity to river water level and river bed water conductivity were established for the 213 Bridge section. The CLM\_RIV model was run at this section to simulate a riparian zone within 3000 m of the southeast riverbank using a horizontal resolution of 60 m. The simulation period covered the whole year of 2012 using a



time step of 1800 s. The atmospheric forcing data were obtained from the China Meteorological Administration Land Data Assimilation System (CLDAS) and developed by the National Meteorological Information Center (NMIC). This high-quality data set combines field observations, remote sensing data and numerical products at a horizontal resolution of 0.0625 degrees. Initial conditions for the simulation were obtained from a 700-year “spin-up” run conducted using the original version of CLM4.5 (without groundwater lateral flow) and cyclically using the CLDAS dataset. We conducted two sensitivity experiments. The first of these examined the sensitivity of the model predictions to changes in the river water level. Four constant river elevations were considered:  $h_r = 1493.1$  m, 1492.1 m, 1491.1 m and 1490.1 m. The hydraulic conductivity of the river bed ( $K_r$ ) was fixed at  $7.4 \text{ m d}^{-1}$ . The second experiment tested the sensitivity of the model to changes in the hydraulic conductivity of the river bed. In this experiment, the boundary condition of the river water level was fixed at  $h_r = 1491.1$  m and four sets of river hydraulic conductivities were prescribed:  $K_r = 3 \text{ m d}^{-1}$ ,  $6 \text{ m d}^{-1}$ ,  $12 \text{ m d}^{-1}$  and  $24 \text{ m d}^{-1}$ .

Then to investigate the eco-hydrological effects of stream-aquifer interaction, a “realistic” simulation and a “control” simulation using CLM\_RIV were conducted. The realistic simulation (called TEST) reproduced processes of stream-aquifer interaction and groundwater lateral flow; the control simulation (called CTL) did not take the stream-aquifer interaction into consideration. Each simulation covered a period of a whole hydrological year from 1 July 2012 to 30 June 2013 using a time step of 1800 s. The models were run at the five sections to simulate both sides of the river within a distance of 3000 m from the river channel using a horizontal resolution of 60 m. As with the sensitivity tests, atmospheric forcing data were used from CLDAS as developed by NMIC. However, instead of using the default land cover data of CLM4.5 (Oleson et al., 2013) we replaced these with data from the M1CLCover land cover map of the Heihe River Basin developed by Ran et al. (2012).

In the TEST and CTL simulations using CLM\_RIV, the lateral hydraulic conductivity of river bed ( $K_r$ ) was set to  $7.4 \text{ m d}^{-1}$  based on research of Xie and Yuan (2010). The boundary conditions of river water levels ( $h_r$ ) for the five sections were obtained from the data set of the hydrometeorological observation network, which is operated by Heihe Watershed Allied Telemetry Experimental Research (HiWATER, Li et al., 2013; Liu et al., 2015). The observations covered all time periods



of our simulations with a time interval of 0.5 h. Both the TEST and CTL runs began from restart files of the 700-year spin-up conducted for each configuration, cyclically using the atmospheric forcing and observed water level data.

#### 4 Eco-hydrological effects of stream-aquifer water interaction

##### 4.1 Validation

5 First, we validated our model using results from the sensitivity experiments. In the first sensitivity test (described in Sect. 3.2), we varied the river levels while holding river bed water conductivity constant, which showed (Figures 4a–4d) that the groundwater table depth near the river channel is significantly reduced (groundwater table is elevated) as the river water level increases. This is because, as Eq. (1) shows, the higher river water level induces a greater hydraulic gradient, which enhances lateral recharge to the riparian aquifer. The second experiment tested the sensitivity of the model to changes in  
10 the river bed hydraulic conductivity while the holding river level constant. As shown in Figures 4e–4h, although the river hydraulic conductivity ranged widely from 3 m d<sup>-1</sup> to 24 m d<sup>-1</sup>, the groundwater table depth variations were similar for all values of conductivity. This means that the groundwater table along the river channel is not very sensitive to  $K_r$ , compared with  $h_r$ . These results allow us to choose  $K_r$  rather arbitrarily, while values of  $h_r$  must be realistic.

Next, we tested our results from the realistic simulation (TEST) using observed data. First of all, we used observation  
15 data from the eddy covariance (EC) and automatic weather station (AWS) system of the Bajitan Gobi Desert station (Liu et al., 2011; Li et al., 2013), a part of hydrometeorological observation network operated by HiWATER, to validate our simulation. The Bajitan Gobi Desert station is located at 100.3042 °E, 38.9150 °N and an elevation of 1562 m. The station is on the northwest riverbank of the first section (213 Bridge) in our simulation at a distance of approximately 2800 m from the channel. The station contains a 10-m flux tower equipped with a series of EC instruments for flux measurements,  
20 and meteorological instruments for regular weather measurements as well as soil temperature and moisture. The underlying surface of this site is Gobi Desert soil and there are few human activities nearby, which benefitted our validation because anthropogenic effects are not considered in the simulation. Figure 5 shows the daily variations in the observations of surface soil temperature, surface soil moisture, sensible heat flux and latent heat flux at the Bajitan Gobi station against the corresponding simulated values from the TEST run. The initial observation times of the EC and AWS  
25 system were, respectively, 14 August 2012 and 19 September 2012, and there was a successive period near June 2013 with



missing measurements for both sensible and latent heat flux. Figures 5a and 5b show that our model can precisely reproduce the soil temperature throughout the year but yields surface soil moisture predictions that have a significant positive bias in spring and winter. Despite this, CLM\_RIV can generally capture the peak value of soil moisture induced by rain events. Figure 5c shows that our model is credible for sensible heat flux simulation, albeit with underestimation of this parameter in winter. Figure 5d shows that CLM\_RIV also simulates the latent head flux well in the rain season, but gives a negative bias in the arid season. Overall, the TEST simulation demonstrated a good ability of CLM\_RIV to reproduce the observations of important parameters, especially in the wet season when the eco-hydrological effects of stream-aquifer water interaction are dominant.

Next, we tested the ability of our model to simulate the groundwater table, which is a key factor in ecological and hydrological effects. We compared the results from both the TEST and CTL simulations with groundwater head data from observation wells distributed over the middle reaches of the Heihe River Basin (Zhou et al., 2013). There were 46 wells within our simulation domain of the five sections. Figure 6 shows the annual values of our simulated groundwater head from both TEST and CTL runs against the observed groundwater heads at the 46 wells. As shown, if the stream-aquifer water transfer is not accounted (as in the CTL run), there is a significant underestimation of water head at nearly all sites. When river-groundwater exchange is considered (as in the TEST simulation), the negative biases are much reduced because the water transfer raises the water table, and the modeled groundwater levels are very close to the observations for most wells. However, there are still a few meters of deviation between TEST simulated levels and observed levels, which indicates the need for further development of our model in the future.

Next, we checked the model's ability to simulate spatial variability by comparing simulated ground temperature from the TEST run with high-resolution remote sensing data from the Advanced Spaceborne Thermal Emission and Reflection Radiometer (ASTER) launched by the United States National Aeronautics and Space Administration (Tachikawa et al., 2011). The ASTER data had been post-processed for the Heihe River Basin by Li et al. (2014). Ground temperature measurements at 90-m resolution were available for five satellite transit events during the summer of 2012. We used relative temperature of the nearest grid to the stream to emphasize spatial variability. The northwest riverbank of the 213 Bridge station was chosen for our comparison because human activities could be neglected there. Figure 7 shows that in



four of the five events our model successfully simulated the increase in ground temperature as distance from the channel increases. However, in the fourth event, the spatial variability predicted by the TEST simulation is much lower than that indicated by ASTER data. This may be caused by the fact that ASTER data are not processed with a cloud mask, which causes overestimation of the cooling effects of streamflow on a cloudy day (Li et al., 2014).

## 5 **4.2 Eco-hydrological effects of stream-aquifer water interaction**

### **4.2.1 Intra-annual responses to river water level**

First, we examined the inter-annual responses of eco-hydrological characteristics to river water level variations. Figure 8 shows the intra-annual variations (at 0.5-h intervals) of water heads at 30 m, 90 m, 210 m and 450 m from the channel on the left riverbanks of streams at the five stations, as well as the observed river water levels. As shown, the 30-m water heads are tightly connected with river levels and have slightly lower elevations and change-frequencies. The 90-m water heads also follow the river level fluctuations but with some time lags, and the elevations are much lower than the river levels and more resistant to change. At 210 m and 450 m from the stream, there is no discernable relation between water table heads and river water levels, and the former are very stable within the year. This means the region that can receive the intra-annual signal of river level changes by stream-aquifer interaction is restricted within a limited distance from the channel, and the response to this signal is stronger closer to the river than farther away. The time correlation coefficients between groundwater tables across the left riverbanks and the river levels of the five sections are plotted in Figure 9. Considering the time lags of the signal transduction, we used the maximum value of cross-correlation coefficients with time lags from 0 to 3 months (at 0.5-h intervals). The standard line where the correlation coefficient passes the 95% confidence level of the Student's t test is also plotted in Figure 9. As shown in Figure 9, the correlation coefficients between the groundwater tables and river levels are more than 0.9 for locations very near to streams, but decrease rapidly as distances from channels increase. The left riverbanks of the 213 Bridge and Pingchuan Bridge stations are least impacted by intra-annual river fluctuations; only at locations within 200 m from streams at these stations do correlation coefficients pass the Student's t test. The most affected riverbank is located at Tielu Bridge station, where intra-annual river level fluctuations influence the water table elevations as far as 450 m from the stream. Nonetheless, the area impacted by intra-annual river water level fluctuations (i.e., a zone within 450 m of a stream) is much smaller than that impacted by



stream-aquifer exchange (i.e., a zone extending to 1800 m from a stream).

We then examined the responses of other eco-hydrological characteristics to intra-annual river water level changes. To highlight the outcomes, we show the simulation results at two rather contrasting stations, Tielu Bridge and 213 Bridge; these stations demonstrated the longest and shortest propagation distances, respectively, for river level fluctuation (Figure 9). We plot the area-averaged data within a 300-m range from both sides of the streams.

Figure 10 shows the time series of selected daily ecological and hydrological variables predicted by TEST and CTL simulations, as well as the river levels and precipitation within the simulation period for the Tielu Bridge section. Figures 10c and 10d show that the effects of stream-aquifer interaction on surface soil water and surface ice, respectively, are dominant in spring, autumn, and winter. As expected, the effects on surface soil ice are especially noticeable in winter, with values predicted by the TEST simulation nearly five times those predicted by CTL. The relative lack of influence of the high river water level of summer (Figure 10a) on soil water seems contradictory, but can be explained by the precipitation variation shown in Figure 10b; in summer, surface soil is wetted most by precipitation and stream water contributes relatively less to this effect, while in other seasons the stream water can significantly affect the surface soil water (and ice) because rain events are sparse. These conclusions can be checked in Figure 10e, which shows that the effects of stream-aquifer interaction are perennially apparent on deep soil water that is much less affected by precipitation.

Figure 10g shows that ground temperature is cooled by stream water in spring and summer and warmed in winter, though the amplitudes of these changes are slight compared with seasonal temperature variation. The higher specific heat capacity induced by wetter soil makes soil temperatures more resistant to the influence of air temperature change than when the soil is dry.

Intra-annual impacts on GPP and ecosystem respiration (RE) are shown in Figures 10h and 10i, respectively. Generally, GPP and RE are both strengthened by stream-aquifer water interaction all year except in winter, and the increased GPP (approximately  $0.03 \text{ mg C m}^{-2} \text{ s}^{-1}$  in the growing season) is higher than RE (approximately  $0.02 \text{ mg C m}^{-2} \text{ s}^{-1}$ ) most of the time. These differences enhance the NEE by approximately  $0.01 \text{ mg C m}^{-2} \text{ s}^{-1}$  in the growing season, which means that riparian plants fix more  $\text{CO}_2$  from May to September than at other times of the year (as Figure 10j shows). However, there is a time period from March to April when RE is enhanced by stream water supplement, while GPP is unaffected. This



time lag causes the riparian vegetation to act as a strong carbon source in this period (Figure 10j) instead of a sink as at other times of the year.

The incremental leaf area index (LAI) and evapotranspiration by water recharge from the river are shown in Figures 10k and 10l, respectively. The LAI is much increased from April to December relative to other times and the stream water supplement can even advance the beginning, and delay the ending, of the growing season for 1–2 months (Figure 10k). Predictions from the TEST simulation indicate that LAI is zero near September 2012, corresponding to the dry river water condition around this time (Figure 10a); this result underlines the high sensitivity of riparian plant growth to the stream-aquifer water interaction. Figure 10l shows that evapotranspiration variability within the year is also highly related to the fluctuation in river level, reemphasizing the key functions of environmental flows for an ecological system.

Figure 11 shows the time series of selected daily ecological and hydrological variables predicted by TEST and CTL simulations, as well as the river levels and precipitation within the simulation period for the 213 Bridge section. The conclusions based on TEST and CTL simulations for Tielu Bridge are generally applicable to the section at 213 Bridge as shown in Figure 11, which means that the intra-annual responses of eco-hydrological elements to river water level changes are similar at a wide range of sections in this arid region. However, due to the propagation distance of river level fluctuation at the 213 Bridge section being much shorter than at Tielu Bridge (Figure 9), the strength of these hydrological and ecological responses is significantly weaker at 213 Bridge than at Tielu Bridge. The differences can be observed by comparing Figures 10 and 11.

#### 4.2.2 Annual averaged effects of stream-aquifer water interaction

After studying the intra-annual responses of the riparian eco-hydrological system to river water fluctuation, we examined the annual averaged effects of stream-aquifer water interaction on riparian eco-hydrological elements.

Figure 12 shows the differences of annual water head between predictions from TEST and CTL simulations along the five sections. All sections show stronger effects of elevated water tables closer to the stream than farther away. The water exchange from stream to aquifer can increase the water head at the grid nearest to the stream (30 m from the channel) by 13 m to 22 m. Furthermore, all cross-sections show water table elevations increased by more than 8 m even at sites nearly 2 km from channels. When averaged for the area within 1800 m from either side of the river channel, the groundwater



tables rose by approximately 10–20 m at the five sections. These results show that the effects of stream-aquifer water interaction on annual averaged groundwater levels can spread very far by groundwater lateral flow. Thus groundwater studies must consider the impacts of water exchange between a riverbank and river, a point also stressed by other researchers (Miguez-Macho et al., 2007; Chen et al., 2010; Di et al., 2011).

5 Figure 13 shows the differences of summer and winter soil moisture (both liquid water and ice are included) predicted by TEST and CTL simulations along the five sections. Predictions at two depths (2 cm and 100 cm) are chosen to represent the surface and deep soil layers, respectively. Figures 13a–13e show that in summer, the deep soil moisture is increased by stream water from  $0.08 \text{ m}^3 \text{ m}^{-3}$  to  $0.16 \text{ m}^3 \text{ m}^{-3}$  at the grid closest to the channel, and that this wetting effect is weaker as the distance from the river increases. Averaged for the region within 1 km from the stream, the deep soil is wetted by river  
10 water by approximately  $0.05 \text{ m}^3 \text{ m}^{-3}$  (a 30% increase) at the riverbank. However, the surface soil moisture is nearly unaffected by stream-aquifer interaction because in summer, surface soil moisture is dominated by precipitation and stream water contributes little to the soil moisture changes. This conclusion is verified in Figures 13f–13j. In winter when rain events are sparse, the wetting effects of stream-aquifer interaction on surface soil moisture are apparent at all sections, though the magnitudes are small (only approximately  $0.02 \text{ m}^3 \text{ m}^{-3}$ , a 10% increase) compared with the wetting effects on  
15 deep soil. Wetter soil supplies more water for riparian plant growth and subsistence than dry soil, especially in the growing season in an arid region, which stresses the necessity of stream-aquifer water interaction in supporting the riparian environment.

The annual averaged ecological effects of stream-aquifer water interaction were also evaluated. Figure 14 shows differences in predicted GPP, RE (both autotrophic and heterotrophic respiration are included) and NEE resulting from  
20 TEST and CTL simulations for the summer period. Because there is no vegetation on the northwest (right) side of the 213 Bridge station, all the values are zero (Figure 14a). Figure 14 shows that GPP and RE increased as the distance to the channel decreased, while NEE increased (with the ecosystem tending to be a carbon sink) by  $0.002\text{--}0.005 \text{ mg C m}^{-2} \text{ s}^{-1}$  (100–300%). The impacts are evident within a range of approximately 1 km. The strongest effects appeared at Tielu Bridge station with increases of more than  $0.05 \text{ mg C m}^{-2} \text{ s}^{-1}$  for GPP and  $0.04 \text{ mg C m}^{-2} \text{ s}^{-1}$  for RE, and a decrease of about  $0.01$   
25  $\text{mg C m}^{-2} \text{ s}^{-1}$  for NEE at the grid nearest to the stream. The influences of stream-aquifer interaction on GPP are stronger



than they are on RE at all sections; this difference explains why the stream effects on NEE are negative (carbon sink) and means that riparian vegetation can absorb more CO<sub>2</sub> and grow better when it is closer to the river. These results highlight the maintenance function of stream-aquifer water interaction for a riparian ecosystem, especially in an arid region.

The simulated effects of stream-aquifer interaction on LAI and canopy transpiration (canopy evaporation is also included) in the summer period are provided in Figure 15. Differences in LAI and transpiration predicted by the TEST and CTL simulations show similar spatial patterns at all sections; in close proximity to the river, LAI and transpiration are increased by supplemental water from the stream. The impacted areas are also within approximately 1 km from the channel for most riverbanks. Averaged over the affected area, the transpiration is enhanced by 0.2–1.0 mm d<sup>-1</sup> (about 100–200%) and LAI is increased by 0.2–1 in summer. The strongest affected section is Tielu Bridge where the LAI and canopy transpiration increased by approximately 5.0 mm d<sup>-1</sup> and 4 mm d<sup>-1</sup>, respectively, at the closest grid to the stream (Figure 15c); riverbanks of other sections are less impacted. The similar spatial distributions of LAI and transpiration across riverbanks means that in this arid region, transpiration along the river is mainly controlled by LAI, which will benefit from stream water lateral infiltration. This finding again stresses the essential influence of stream-aquifer water interaction in riparian hydrologic and carbon cycles, as well as in maintaining environmental integrity.

Lastly, we show the effects of stream-groundwater exchange on vertical energy and water fluxes along a river. Figure 16 shows the differences in sensible heat (SH) and latent heat (LH) fluxes predicted by the TEST and CTL simulations for summer and winter. Figures 16a–16e show that the effects on SH and LH in summer display opposite trends along the riverbanks: LH becomes stronger closer to the stream while SH becomes weaker. The stronger LH is due to the enhanced evapotranspiration along the river (Figure 15), which also induces weaker SH. However, the SH and LH trends change in winter. Figures 16f–16j show that both SH and LH exhibit small positive changes closer to riverbanks, though the magnitudes are much smaller than they are in summer; this may be induced by the lower river water level in winter (Figure 8). Because SH and LH are key factors influencing the atmosphere above a plant canopy, local weather and climate would also be modified by the effects of stream-aquifer water interaction; this suggests that when studying local climate in areas that include streams, the effects of surface water should not be ignored.



## 5 Conclusions and Discussion

In this study, we incorporated a scheme of stream-aquifer water interaction into the land surface model CLM4.5. After sensitivity tests for selected parameters demonstrated the reliability of the new model (CLM\_RIV), the model was used to make two simulations to detect the effects of stream-aquifer water interaction on ecological and hydrological processes on riparian banks at five different locations. One simulation was “forced” using observed river water levels. The other “control” simulation did not take stream-aquifer water exchange into consideration. Both simulations covered a period from July 2012 to June 2013. Comparisons of simulation outputs and observations from EC and AWS systems, water wells and remote sensing data demonstrated that CLM\_RIV shows considerable ability to reproduce the natural conditions along riverbanks.

10 The main conclusions of this study are as follows. (1) A riparian groundwater table responds to the intra-annual variation in river water level, but the response areas are limited to within 200–450 m from the stream channel. The correlation coefficient between the groundwater table and river level can reach 0.9 at the nearest model grid to the river, but rapidly decreases as the distance from the river increases. Surface soil liquid water in the rain season is less impacted by river level variation than is deep soil water, which follows the river level fluctuation all year. (2) Over a typical riverbank section (Tielu Bridge), averaged GPP and respiration of riparian vegetation within 300 m from the stream increased by approximately  $0.03 \text{ mg C m}^{-2} \text{ s}^{-1}$  and  $0.02 \text{ mg C m}^{-2} \text{ s}^{-1}$ , respectively, in the growing season due to increased soil water, resulting in enhanced NEE of approximately  $0.01 \text{ mg C m}^{-2} \text{ s}^{-1}$ . Evapotranspiration in this zone also increased (by approximately  $3 \text{ mm d}^{-1}$ ). Furthermore, the growing season of riparian vegetation is also extended by 2–3 months due to the sustaining water recharge from the stream, and even a short-term decline in river level can negatively impact LAI near the stream during the growing season. (3) All impacted ecological and hydrological characteristics are restricted to an area within approximately 1 km from the channel, and the effects become stronger as distance to the river decreases. These conclusions highlight the functions of stream-aquifer water interaction on sustaining and controlling the riparian ecological system, and indicate the potential benefits of water regulation, such as through artificial stream water conveyance, to maintain stream flow.

25 However, there are assumptions and limitations of this study that should be noted. Besides the intrinsic uncertainties of



CLM and atmospheric forcing (Bonan et al., 2011, 2013; Mao et al., 2012; Wang et al., 2013), the parameters reflecting the land and river conditions in our scheme, such as  $K_j$ ,  $K_r$  and  $f$  in Eq. (4)–(14), are highly parameterized based on some simple assumptions to facilitate data collection and computation, while the real states of geological structures and sediment-bedrock profiles are so complex that they are almost impossible to describe accurately. However, the sensitivity experiments and comparison of our results with data from multiple sources (Sect. 4.1) prove that these uncertainties do not significantly affect the simulation ability of CLM\_RIV. Another restriction on our results is that human activities, such as irrigation that may take place on riverbanks, are not considered in our model. Such activities could cause our results to deviate considerably from the real situation. Arguably, the aim of this study was to emphasize the effects of stream-aquifer water interaction (which is a totally natural process) on riparian eco-hydrological processes. Thus, ignoring anthropogenic disturbances on riverbanks (such as crop cultivation, irrigation and water diversion), which may interfere with the natural influences we simulated, was a reasonable approach in this research.

Some future studies are also needed. To overcome the uncertainties of parameterization, more systematic experiments to test the sensitivity of model parameters should be conducted, and corresponding observations or more sophisticated estimation approaches for key parameters relating to stream-aquifer interaction are needed. Applying our model to other typical regions (even at a global scale) having different climatic and hydrological environments is expected. Finally a land-river-atmosphere interaction model that can simulate the water and energy exchange between each component is needed for studying the more comprehensive effects of stream water flows.

**Acknowledgements** This study was supported by the National Natural Science Foundation of China (Grants 91125016 and 41575096) and by the Chinese Academy of Sciences Strategic Priority Research Program under Grant XDA05110102. We would like to thank Xing Yuan, Xiangjun Tian and Yuanyaun Wang for their assistance with this work and helpful discussion.



## References

- Arnold, J., Muttiyah, R. S., Srinivasan, R., and Allen, P.: Regional estimation of base flow and groundwater recharge in the Upper Mississippi river basin, *J Hydrol*, 227, 21-40, 2000.
- Baskaran, S., Ransley, T., Brodie, R., and Baker, P.: Investigating groundwater–river interactions using environmental tracers, *Australian Journal of Earth Sciences*, 56, 13-19, 2009.
- 5 Bear, J.: *Dynamics of Fluids in Porous Media*, 1972.
- Bonan, G. B., Hartman, M. D., Parton, W. J., and Wieder, W. R.: Evaluating litter decomposition in earth system models with long - term litterbag experiments: an example using the Community Land Model version 4 (CLM4), *Global change biology*, 19, 957-974, 2013.
- 10 Bonan, G. B., Lawrence, P. J., Oleson, K. W., Levis, S., Jung, M., Reichstein, M., Lawrence, D. M., and Swenson, S. C.: Improving canopy processes in the Community Land Model version 4 (CLM4) using global flux fields empirically inferred from FLUXNET data, *Journal of Geophysical Research: Biogeosciences (2005–2012)*, 116, 2011.
- Chen, F., and Xie, Z. H.: Effects of interbasin water transfer on regional climate: A case study of the Middle Route of the South-to-North Water Transfer Project in China, *J Geophys Res-Atmos*, 115, Artn D11112, Doi
- 15 10.1029/2009jd012611, 2010.
- Chen, F., and Xie, Z. H.: Effects of crop growth and development on regional climate: a case study over East Asian monsoon area, *Clim Dynam*, 38, 2291-2305, 10.1007/s00382-011-1125-y, 2012.
- Chen, Y., Zhang, D. Q., Sun, Y. B., Liu, X. N., Wang, N. Z., and Savenije, H. H. G.: Water demand management: A case study of the Heihe River Basin in China, *Phys Chem Earth*, 30, 408-419, 10.1016/j.pce.2005.06.019, 2005.
- 20 Chen, Y. N., Chen, Y. P., Xu, C. C., Ye, Z. X., Li, Z. Q., Zhu, C. G., and Ma, X. D.: Effects of ecological water conveyance on groundwater dynamics and riparian vegetation in the lower reaches of Tarim River, China, *Hydrol Process*, 24, 170-177, 10.1002/hyp.7429, 2010.
- Chen, Y. N., Zhang, X. L., Zhu, X. M., Li, W. H., Zhang, Y. M., Xu, H. L., Zhang, H. F., and Chen, Y. P.: Analysis on the ecological benefits of the stream water conveyance to the dried-up river of the lower reaches of Tarim River, China,
- 25 *Sci China Ser D*, 47, 1053-1064, 10.1360/03yd0101, 2004.



- Di, Z. H., Xie, Z. H., Yuan, X., Tian, X. J., Luo, Z. D., and Chen, Y. N.: Prediction of water table depths under soil water-groundwater interaction and stream water conveyance, *Sci China Earth Sci*, 54, 420-430, DOI 10.1007/s11430-010-4050-8, 2011.
- Fan, Y.: Groundwater in the Earth's critical zone: Relevance to large-scale patterns and processes, *Water Resour Res*, 51, 3052-3069, 10.1002/2015WR017037, 2015.
- 5
- Fan, Y., and Miguez-Macho, G.: Potential groundwater contribution to Amazon evapotranspiration, *Hydrol Earth Syst Sc*, 14, 2039-2056, 10.5194/hess-14-2039-2010, 2010.
- Fan, Y., and Miguez-Macho, G.: A simple hydrologic framework for simulating wetlands in climate and earth system models, *Clim Dynam*, 37, 253-278, 10.1007/s00382-010-0829-8, 2011.
- 10
- Fan, Y., Miguez-Macho, G., Weaver, C. P., Walko, R., and Robock, A.: Incorporating water table dynamics in climate modeling: 1. Water table observations and equilibrium water table simulations, *J Geophys Res-Atmos*, 112, ArtID10125, 10.1029/2006jd008111, 2007.
- Gent, P. R., Danabasoglu, G., Donner, L. J., Holland, M. M., Hunke, E. C., Jayne, S. R., Lawrence, D. M., Neale, R. B., Rasch, P. J., Vertenstein, M., Worley, P. H., Yang, Z. L., and Zhang, M. H.: The Community Climate System Model Version 4, *J Climate*, 24, 4973-4991, Doi 10.1175/2011jcli4083.1, 2011.
- 15
- Hurrell, J. W., Holland, M. M., Gent, P. R., Ghan, S., Kay, J. E., Kushner, P. J., Lamarque, J. F., Large, W. G., Lawrence, D., Lindsay, K., Lipscomb, W. H., Long, M. C., Mahowald, N., Marsh, D. R., Neale, R. B., Rasch, P., Vavrus, S., Vertenstein, M., Bader, D., Collins, W. D., Hack, J. J., Kiehl, J., and Marshall, S.: The Community Earth System Model A Framework for Collaborative Research, *B Am Meteorol Soc*, 94, 1339-1360, Doi 10.1175/Bams-D-12-00121.1, 2013.
- 20
- Li, H., Sun, D., Yu, Y., Wang, H., Liu, Y., Liu, Q., Du, Y., Wang, H., and Cao, B.: Evaluation of the VIIRS and MODIS LST products in an arid area of Northwest China, *Remote Sensing of Environment*, 142, 111-121, 2014.
- Li, X., Cheng, G. D., Liu, S. M., Xiao, Q., Ma, M. G., Jin, R., Che, T., Liu, Q. H., Wang, W. Z., Qi, Y., Wen, J. G., Li, H. Y., Zhu, G. F., Guo, J. W., Ran, Y. H., Wang, S. G., Zhu, Z. L., Zhou, J., Hu, X. L., and Xu, Z. W.: Heihe Watershed



- Allied Telemetry Experimental Research (HiWATER): Scientific Objectives and Experimental Design, *B Am Meteorol Soc*, 94, 1145-1160, 10.1175/Bams-D-12-00154.1, 2013.
- Li, X., Lu, L., Cheng, G. D., and Xiao, H. L.: Quantifying landscape structure of the Heihe River Basin, north-west China using FRAGSTATS, *J Arid Environ*, 48, 521-535, DOI 10.1006/jare.2000.0715, 2001.
- 5 Liang, X., and Xie, Z. H.: Important factors in land-atmosphere interactions: surface runoff generations and interactions between surface and groundwater, *Global Planet Change*, 38, 101-114, 10.1016/S0921-8181(03)00012-2, 2003.
- Liang, X., Xie, Z. H., and Huang, M. Y.: A new parameterization for surface and groundwater interactions and its impact on water budgets with the variable infiltration capacity (VIC) land surface model, *J Geophys Res-Atmos*, 108, ArtId 8613, 10.1029/2002jd003090, 2003.
- 10 Lindsay, K., Bonan, G. B., Doney, S. C., Hoffman, F. M., Lawrence, D. M., Long, M. C., Mahowald, N. M., Moore, J. K., Randerson, J. T., and Thornton, P. E.: Preindustrial-Control and Twentieth-Century Carbon Cycle Experiments with the Earth System Model CESM1(BGC), *J Climate*, 27, 8981-9005, Doi 10.1175/Jcli-D-12-00565.1, 2014.
- Liu, J., Chen, R., Song, Y., Yang, Y., Qing, W., Han, C., and Liu, Z.: Observations of precipitation type using a time-lapse camera in a mountainous region and calculation of the rain/snow proportion based on the critical air temperature,
- 15 *Environ Earth Sci*, 73, 1545-1554, 10.1007/s12665-014-3506-0, 2014.
- Liu, S., Xu, Z., Wang, W., Jia, Z., Zhu, M., Bai, J., and Wang, J.: A comparison of eddy-covariance and large aperture scintillometer measurements with respect to the energy balance closure problem, *Hydrol Earth Syst Sc*, 15, 1291-1306, 2011.
- Lu, L., Li, X., and Cheng, G. D.: Landscape evolution in the middle Heihe River Basin of north-west China during the last
- 20 decade, *J Arid Environ*, 53, 395-408, 10.1006/jare.2002.1032, 2003.
- Mao, J., Thornton, P. E., Shi, X., Zhao, M., and Post, W. M.: Remote Sensing Evaluation of CLM4 GPP for the Period 2000-09\*, *J Climate*, 25, 5327-5342, 2012.
- Maxwell, R. M., Chow, F. K., and Kollet, S. J.: The groundwater-land-surface-atmosphere connection: Soil moisture effects on the atmospheric boundary layer in fully-coupled simulations, *Adv Water Resour*, 30, 2447-2466,
- 25 10.1016/j.advwatres.2007.05.018, 2007.



- Maxwell, R. M., and Kollet, S. J.: Interdependence of groundwater dynamics and land-energy feedbacks under climate change, *Nat Geosci*, 1, 665-669, Doi 10.1038/Ngeo315, 2008.
- Miguez-Macho, G., Fan, Y., Weaver, C. P., Walko, R., and Robock, A.: Incorporating water table dynamics in climate modeling: 2. Formulation, validation, and soil moisture simulation, *J Geophys Res-Atmos*, 112, Artn D13108, 10.1029/2006jd008112, 2007.
- 5 Oleson, K., Lawrence, D., Bonan, G., Drewniak, B., Huang, M., Koven, C., Levis, S., Li, F., Riley, W., and Subin, Z.: Technical Description of version 4.5 of the Community Land Model (CLM), NCAR, National Center for Atmospheric Research (NCAR) Boulder, Colorado, 2013.
- Qi, S. Z., and Luo, F.: Water environmental degradation of the Heihe River Basin in arid northwestern China, *Environ Monit Assess*, 108, 205-215, 10.1007/s10661-005-3912-6, 2005.
- 10 Ran, Y., Li, X., Lu, L., and Li, Z.: Large-scale land cover mapping with the integration of multi-source information based on the Dempster–Shafer theory, *International Journal of Geographical Information Science*, 26, 169-191, 2012.
- Scanlon, B. R., Healy, R. W., and Cook, P. G.: Choosing appropriate techniques for quantifying groundwater recharge, *Hydrogeol J*, 10, 18-39, 2002.
- 15 Tachikawa, T., Kaku, M., Iwasaki, A., Gesch, D., Oimoen, M., Zhang, Z., Danielson, J., Krieger, T., Curtis, B., and Haase, J.: ASTER Global Digital Elevation Model Version 2—Summary of Validation Results, ASTER GDEM Validation Team ([http://www.jspacesystems.or.jp/ersdac/GDEM/ver2Validation/Summary\\_GDEM2\\_validation\\_report\\_final.pdf](http://www.jspacesystems.or.jp/ersdac/GDEM/ver2Validation/Summary_GDEM2_validation_report_final.pdf)), 2011.
- Wang, K., Mao, J., Dickinson, R. E., Shi, X., Post, W. M., Zhu, Z., and Myneni, R. B.: Evaluation of CLM4 solar radiation partitioning scheme using remote sensing and site level FPAR datasets, *Remote Sensing*, 5, 2857-2882, 2013.
- 20 Wu, J. K., Ding, Y., Ye, B., Yang, Q., Zhang, X., and Wang, J.: Spatio-temporal variation of stable isotopes in precipitation in the Heihe River Basin, Northwestern China, *Environ Earth Sci*, 61, 1123-1134, 10.1007/s12665-009-0432-7, 2010.
- Xie, Z. H., Di, Z. H., Luo, Z. D., and Ma, Q.: A Quasi-Three-Dimensional Variably Saturated Groundwater Flow Model for Climate Modeling, *J Hydrometeorol*, 13, 27-46, Doi 10.1175/Jhm-D-10-05019.1, 2012.
- 25



- Xie, Z. H., and Yuan, X.: Prediction of water table under stream-aquifer interactions over an arid region, *Hydrol Process*, 24, 160-169, Doi 10.1002/Hyp.7434, 2010.
- Xie, Z. H., Zeng, N., Wang, H. J., Lin, Z., Tian, X. J., and Jia, B. H.: Past, present and future of the carbon cycle, *Natl Sci Rev*, 1, 18-21, 10.1093/nsr/nwt021, 2014.
- 5 Yu, Y., Xie, Z. H., and Zeng, X. B.: Impacts of modified Richards equation on RegCM4 regional climate modeling over East Asia, *J Geophys Res-Atmos*, 119, 12642-12659, Doi 10.1002/2014jd021872, 2014.
- Zhao, W., and Cheng, G.: Review of several problems on the study of eco-hydrological processes in arid zones, *Chinese Sci Bull*, 47, 353-360, 2002.
- Zhou, J., Hu, B. X., Cheng, G., Wang, G., and Li, X.: Development of a three - dimensional watershed modelling system  
10 for water cycle in the middle part of the Heihe rivershed, in the west of China, *Hydrol Process*, 25, 1964-1978, 2011.
- Zou, J., Xie, Z. H., Yu, Y., Zhan, C. S., and Sun, Q.: Climatic responses to anthropogenic groundwater exploitation: a case study of the Haihe River Basin, Northern China, *Clim Dynam*, 42, 2125-2145, DOI 10.1007/s00382-013-1995-2, 2014.
- Zou, J., Xie, Z. H., Zhan, C. S., Qin, P. H., Sun, Q., Jia, B. H., and Xia, J.: Effects of anthropogenic groundwater  
15 exploitation on land surface processes: A case study of the Haihe River Basin, northern China, *J Hydrol*, 524, 625-641, DOI 10.1016/j.jhydrol.2015.03.026, 2015.



**Table 1** The locations and relevant information about the five selected sections used in simulations.

Number of section	Name	Latitude	Longitude	Width (m)	Riverbank elevation (m)	Bottom elevation (m)	Flow direction
1	213 Bridge	38°54'43.55"N	100°20'41.05"E	330	1493.1	1488.8	Northeast
2	312 Bridge	38°59'51.71"N	100°24'38.76"E	70	1402	1397	Northeast
3	Tielu Bridge	39°2'33.08"N	100°25'49.42"E	50	1382	1379.25	Northeast
4	Pingchuan Bridge	39°20'2.03"N	100°5'49.63"E	130	1323.8	1319	West
5	Gaotai Bridge	39°23'22.93"N	99°49'37.29"E	210	1295.5	1288.5	West

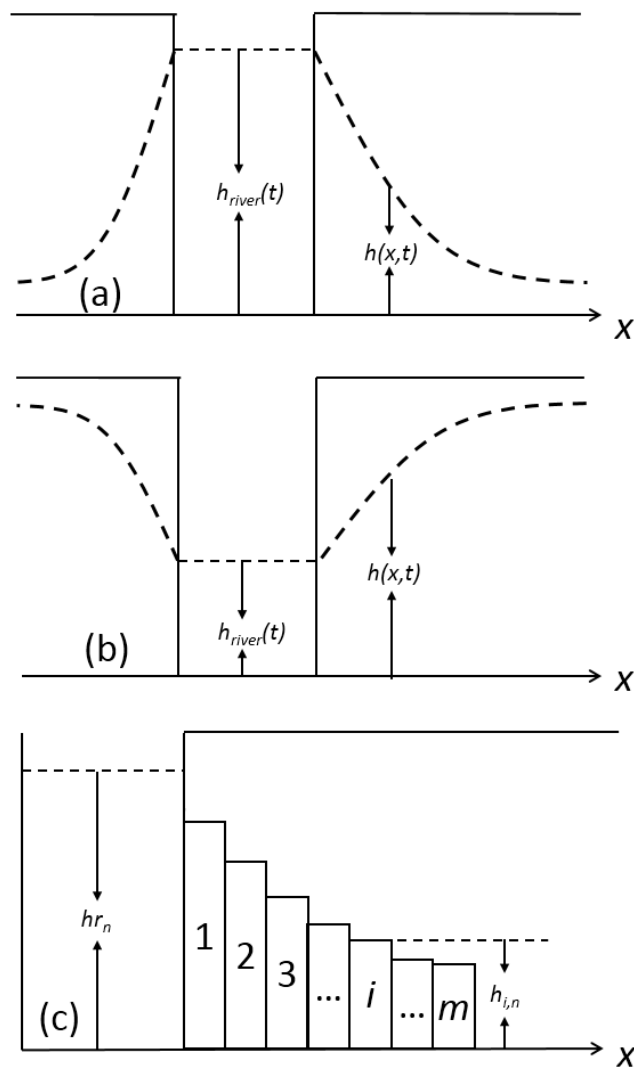


**Figure 1** Schematic representation of stream-aquifer water interaction when (a) the river water level is higher than its neighboring groundwater table and (b) the river water level is lower than its neighboring groundwater table. (c) Schematic diagram for horizontal discrete grid cells of a riverbank.

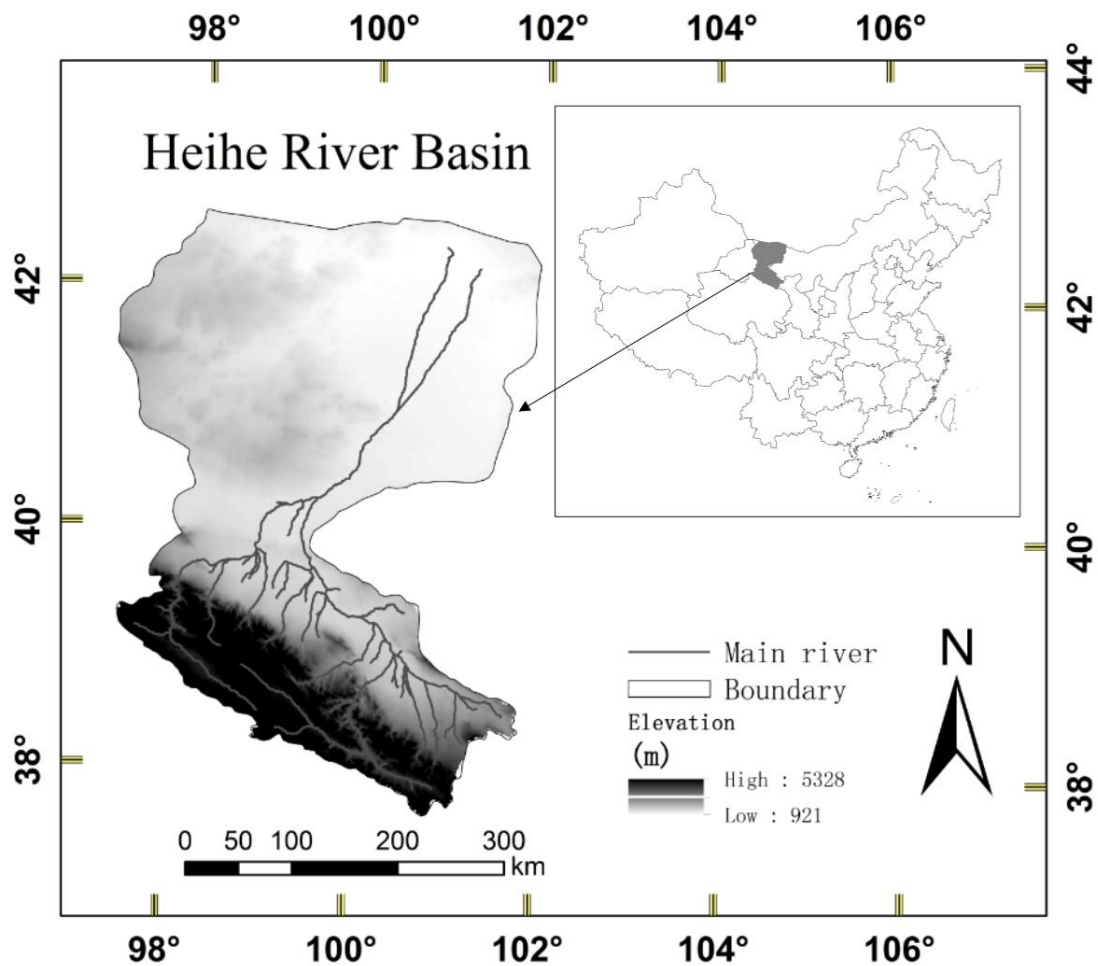


**Figure 2** Study area and location of the Heihe River Basin in northwest China.

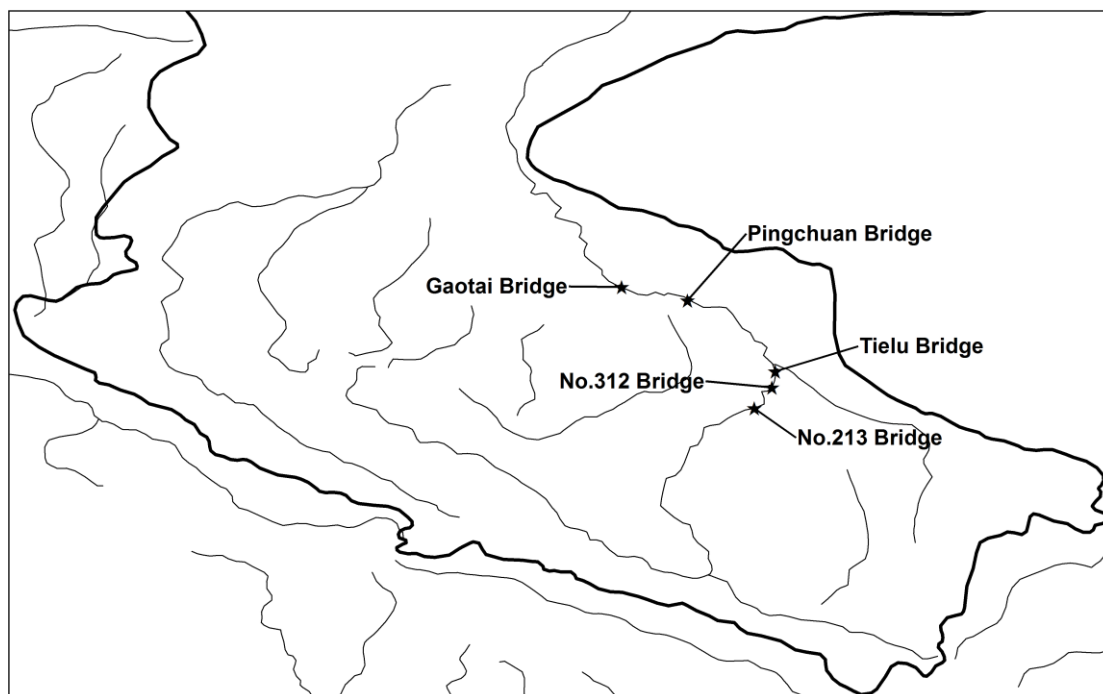


**Figure 3** Locations of the five sections in the middle reaches of the Heihe River that were used for simulations.

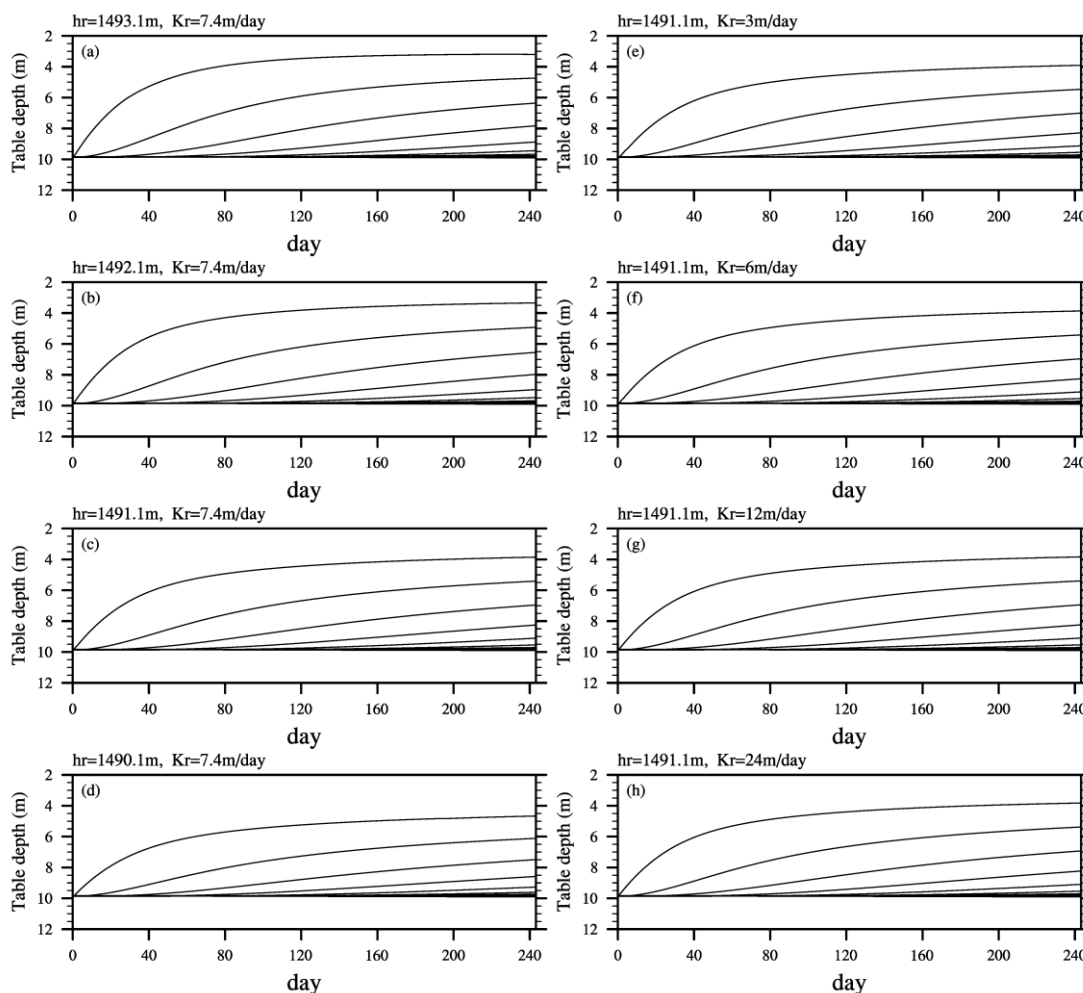


**Figure 4** Sensitivities of the river water level  $h_r$  and river bed hydraulic conductivity  $K_r$ . (a-d) Time series of the simulated groundwater table depths for 20 grid cells in the first sensitivity experiment. (e-h) Time series for the second sensitivity experiment.

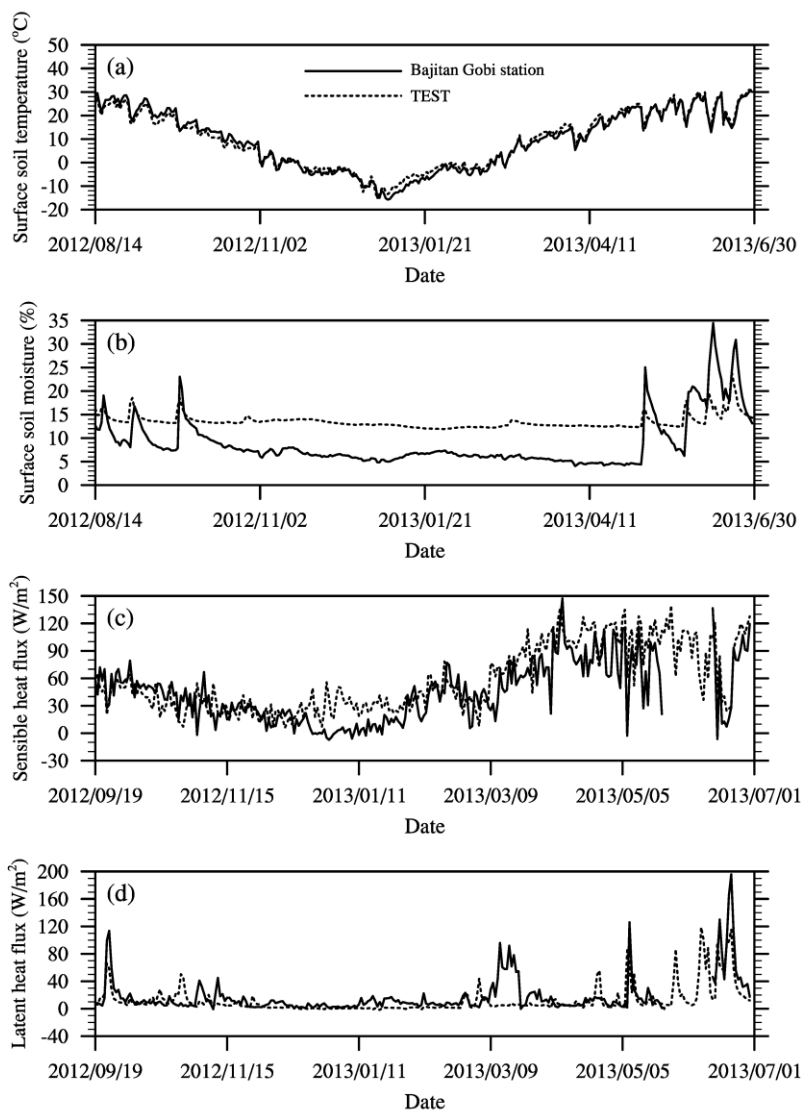


**Figure 5** Time series of the observations from the eddy covariance and automatic weather station systems and results from the TEST simulation at Bajitan Gobi station for (a) surface soil temperature, (b) surface soil moisture, (c) sensible heat flux and (d) latent heat flux.

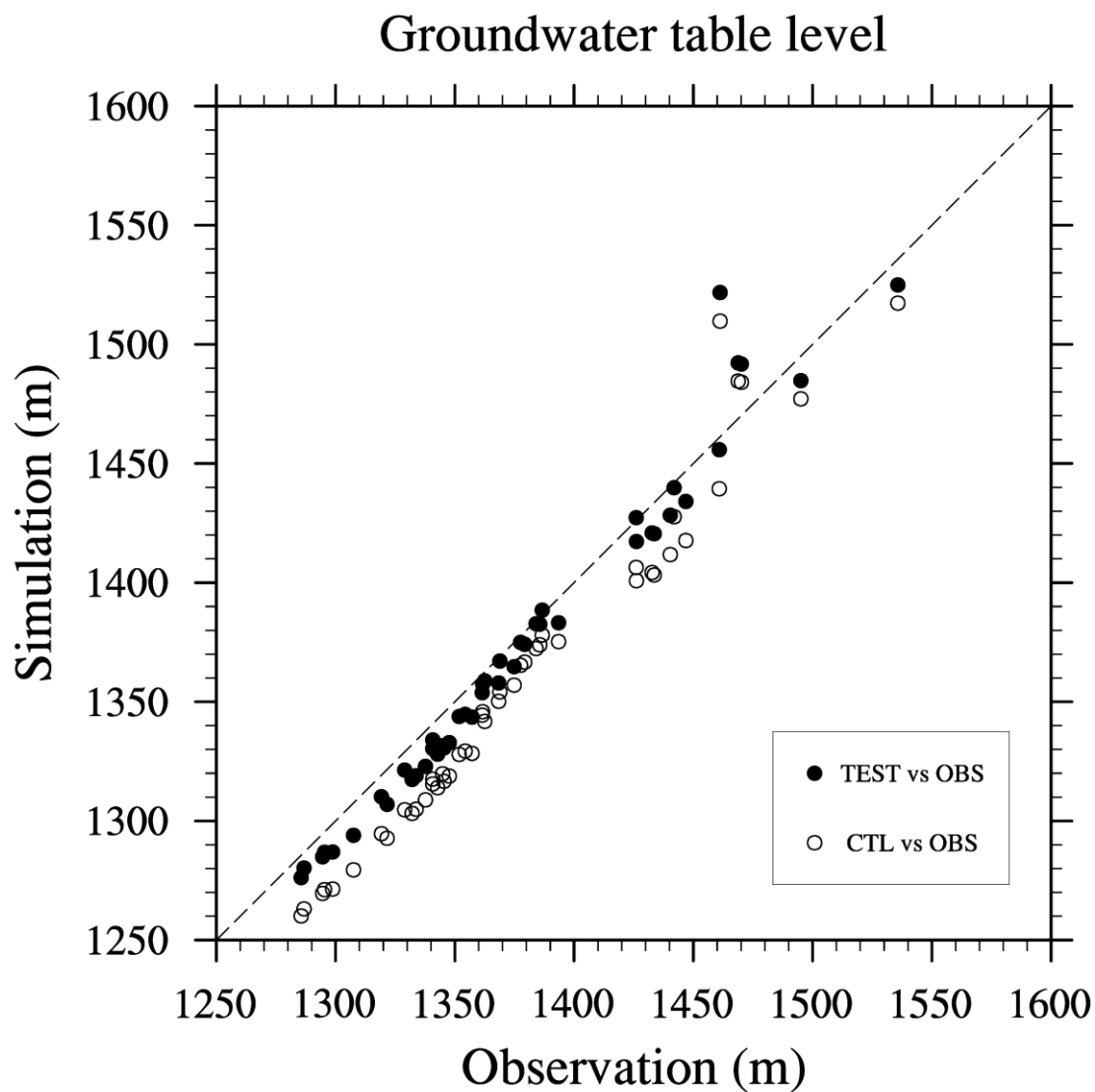


**Figure 6** Annual groundwater head predicted by TEST and CTL simulations against observed climatology water head data from 46 observation wells.

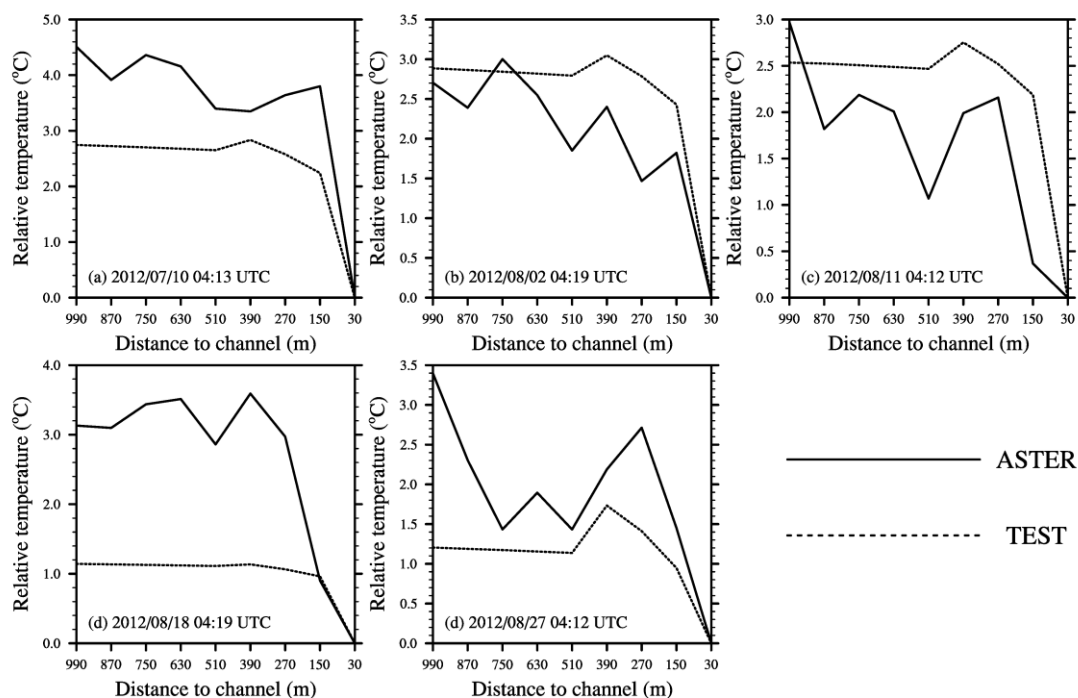


**Figure 7** Relative ground temperature across the left riverbank of the 213 Bridge station from the TEST simulation and corresponding remote sensing data from five ASTER satellite transit events of (a) 2012/07/10 04:13 UTC, (b) 2012/08/02 04:19 UTC, (c) 2012/08/11 04:12 UTC, (d) 2012/08/18 04:19 UTC and (e) 2012/08/27 04:12 UTC.

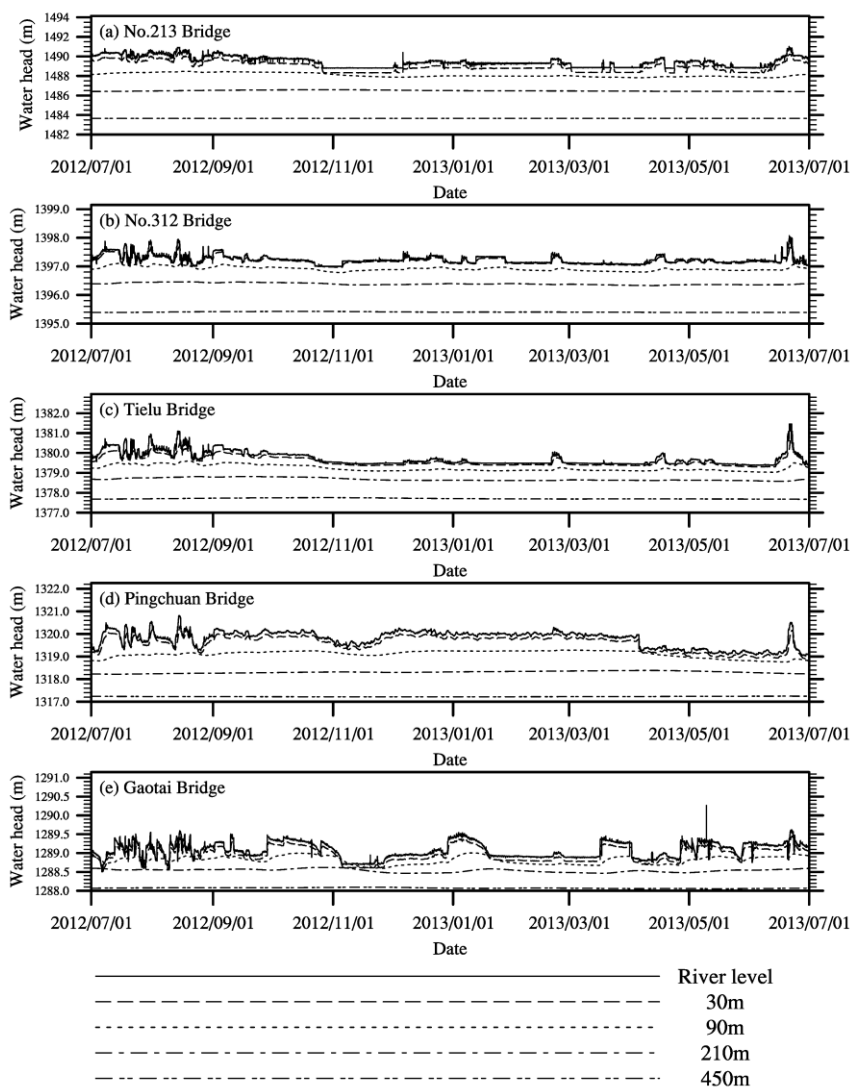


**Figure 8** Time series of simulated water heads at 30 m, 90 m, 210 m and 450 m from streams and the observed river water levels at the five left riverbanks of stations at (a) 213 Bridge, (b) 312 Bridge, (c) Tielu Bridge, (d) Pingchuan Bridge and (e) Gaotai Bridge.

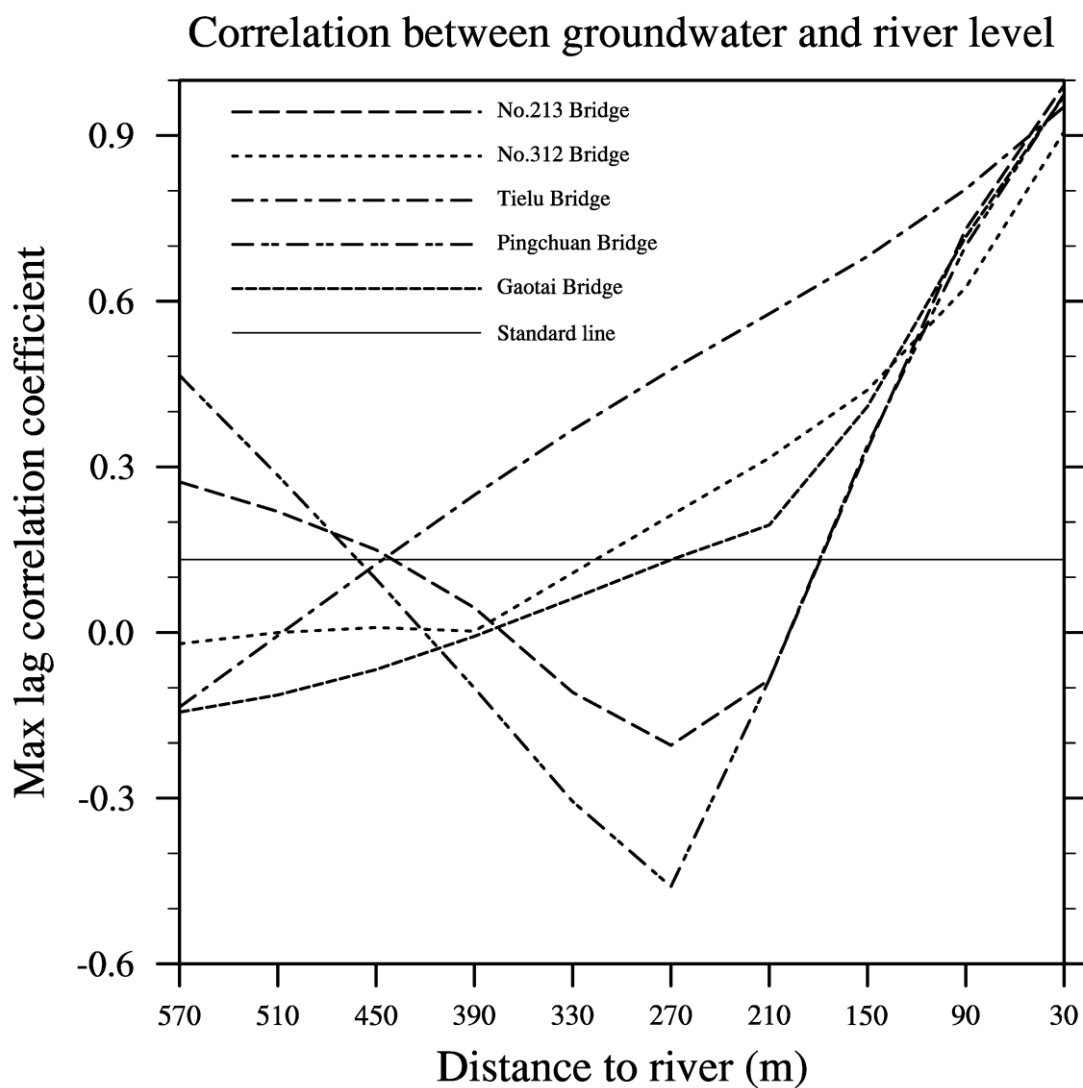


**Figure 9** Maximum lag correlation coefficients between simulated groundwater tables across the left riverbanks and the river water levels at the five stations, and the standard line representing the value of correlation coefficient passing the Student's t test with a confidence level of 95%.

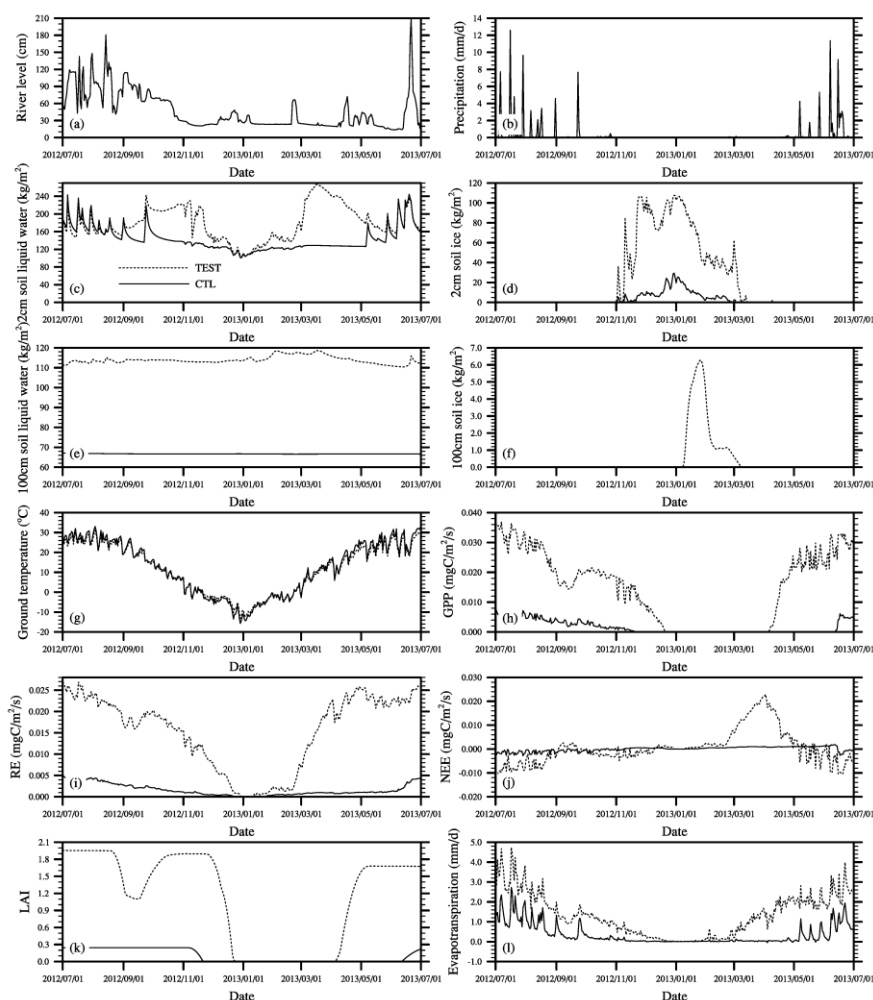


**Figure 10** Time series of area-averaged daily (a) observed river level and (b) observed precipitation, as well as (c) 2-cm soil liquid water, (d) 2-cm soil ice, (e) 100-cm soil liquid water, (f) 100-cm soil ice, (g) ground temperature, (h) gross primary productivity, (i) respiration efficiency, (j) net ecosystem exchange, (k) leaf area index and (l) evapotranspiration predicted by TEST and CTL simulations within 300 m of both sides of the stream at the Tielu Bridge station.

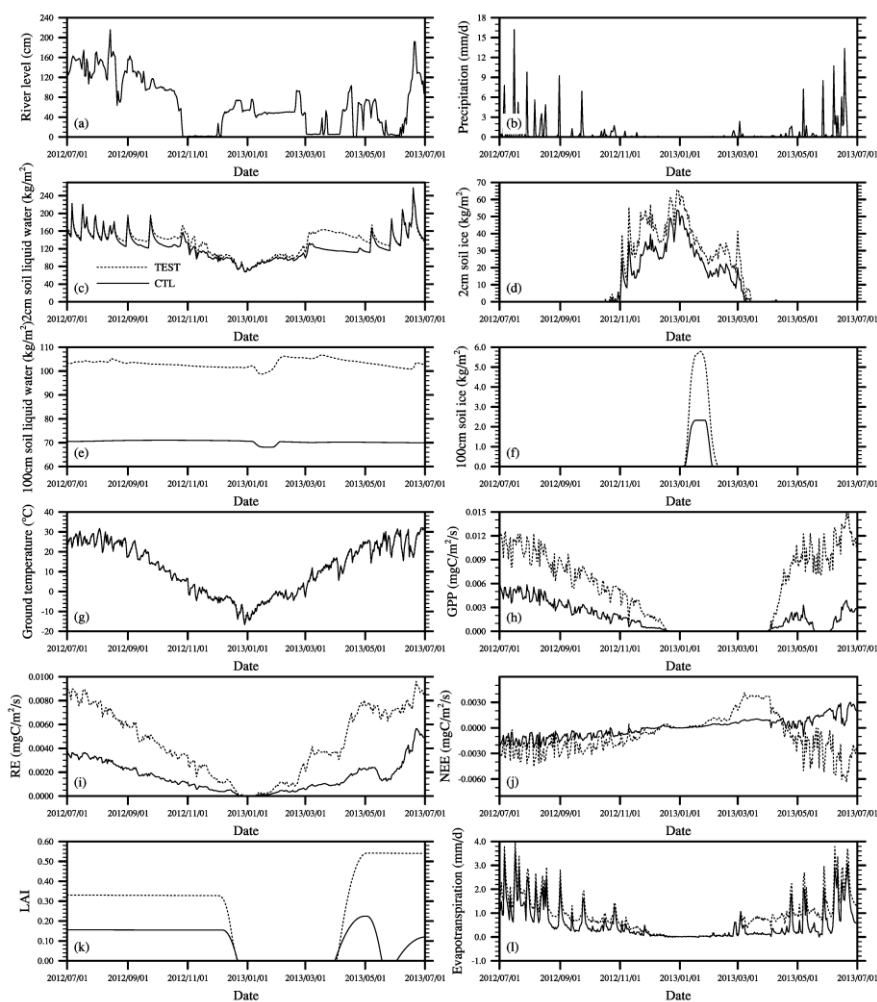


**Figure 11** Time series of area-averaged daily (a) observed river level and (b) observed precipitation, as well as (c) 2-cm soil liquid water, (d) 2-cm soil ice, (e) 100-cm soil liquid water, (f) 100-cm soil ice, (g) ground temperature, (h) gross primary productivity, (i) respiration efficiency, (j) net ecosystem exchange, (k) leaf area index and (l) evapotranspiration predicted by TEST and CTL simulations within 300 m of both sides of the stream at the 213 Bridge station.

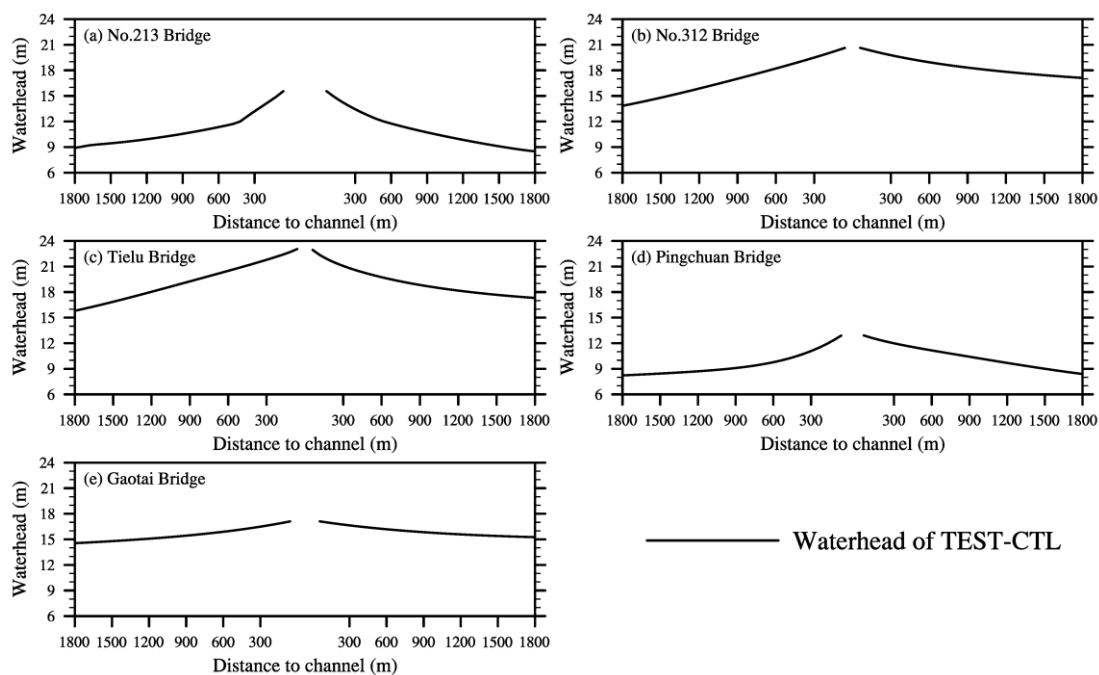


**Figure 12** Differences between annual water heads predicted by TEST and CTL simulations along the five sections at (a) 213 Bridge, (b) 312 Bridge, (c) Tielu Bridge, (d) Pingchuan Bridge and (e) Gaotai Bridge. The discontinuous parts of the curves represent the river areas.

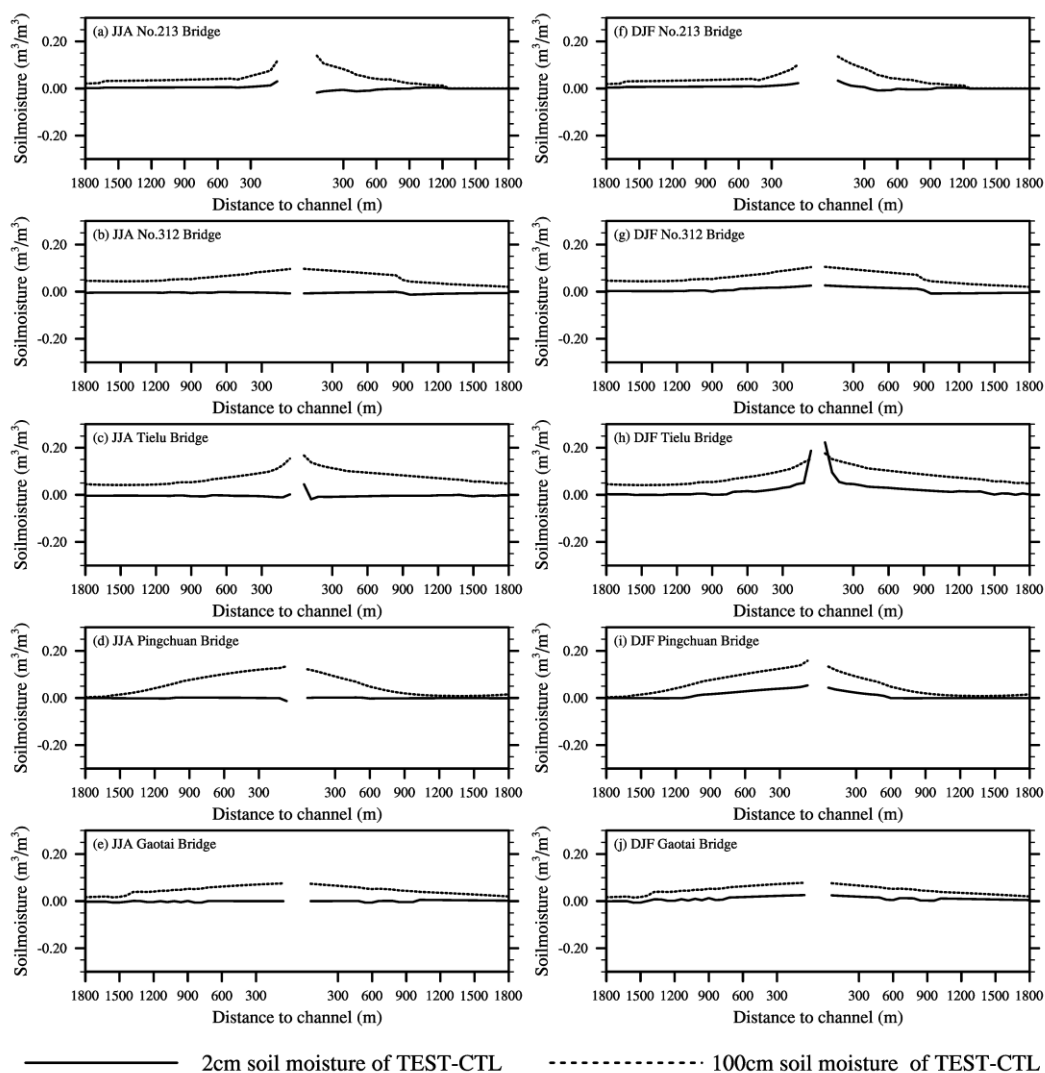


**Figure 13** Differences of (a–e) summer and (f–j) winter soil moisture (both liquid water and ice are included) predicted at depths of 2 cm and 100 cm by TEST and CTL simulations along the five sections at (a and f) 213 Bridge, (b and g) 312 Bridge, (c and h) Tielu Bridge, (d and i) Pingchuan Bridge and (e and j) Gaotai Bridge. The discontinuous parts of the curves represent the river areas.

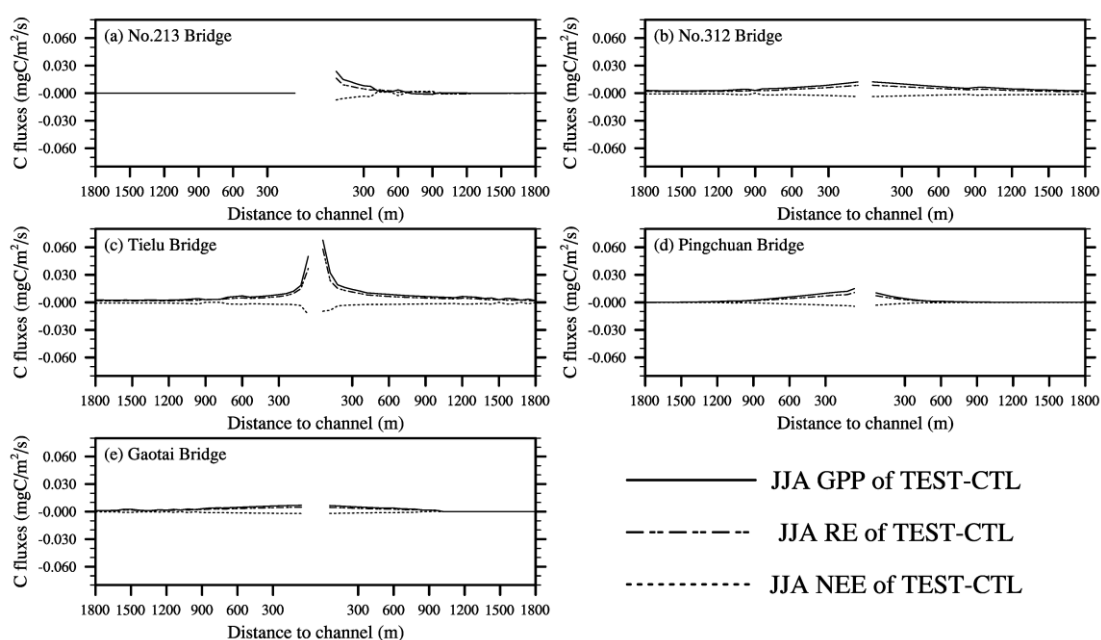


**Figure 14.** Differences between gross primary productivity, respiration efficiency and net ecosystem exchange predicted by TEST and CTL simulations during summer along the five sections at (a) 213 Bridge, (b) 312 Bridge, (c) Tielu Bridge, (d) Pingchuan Bridge and (e) Gaotai Bridge. The discontinuous parts of the curves represent the river areas.

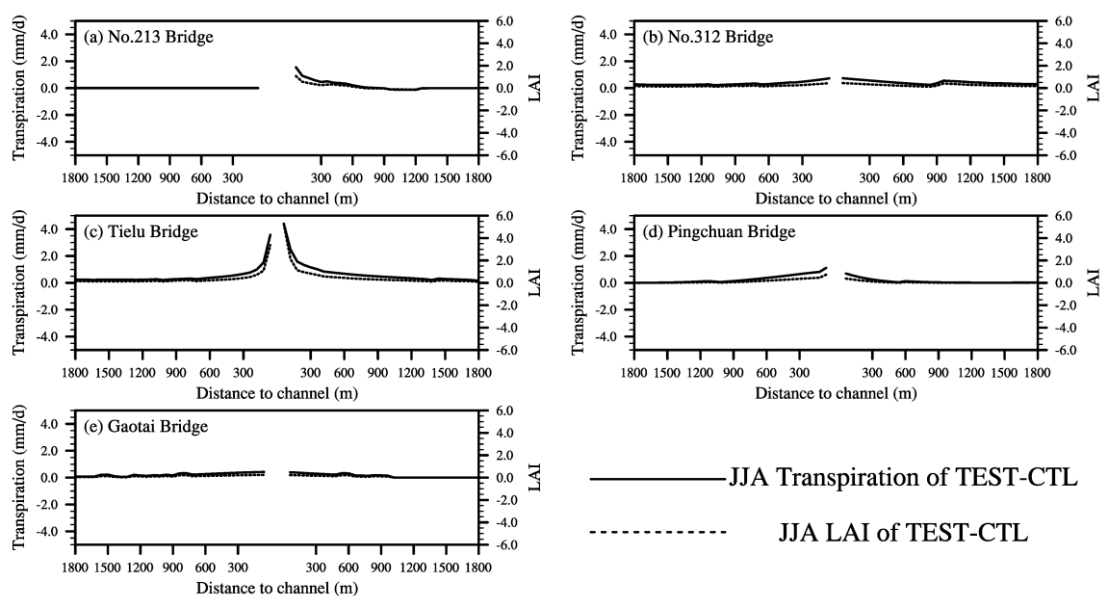


**Figure 15.** Differences between canopy transpiration and leaf area index predicted by TEST and CTL simulations during summer along the five sections at (a) 213 Bridge, (b) 312 Bridge, (c) Tielu Bridge, (d) Pingchuan Bridge and (e) Gaotai Bridge. The discontinuous parts of the curves represent the river areas.

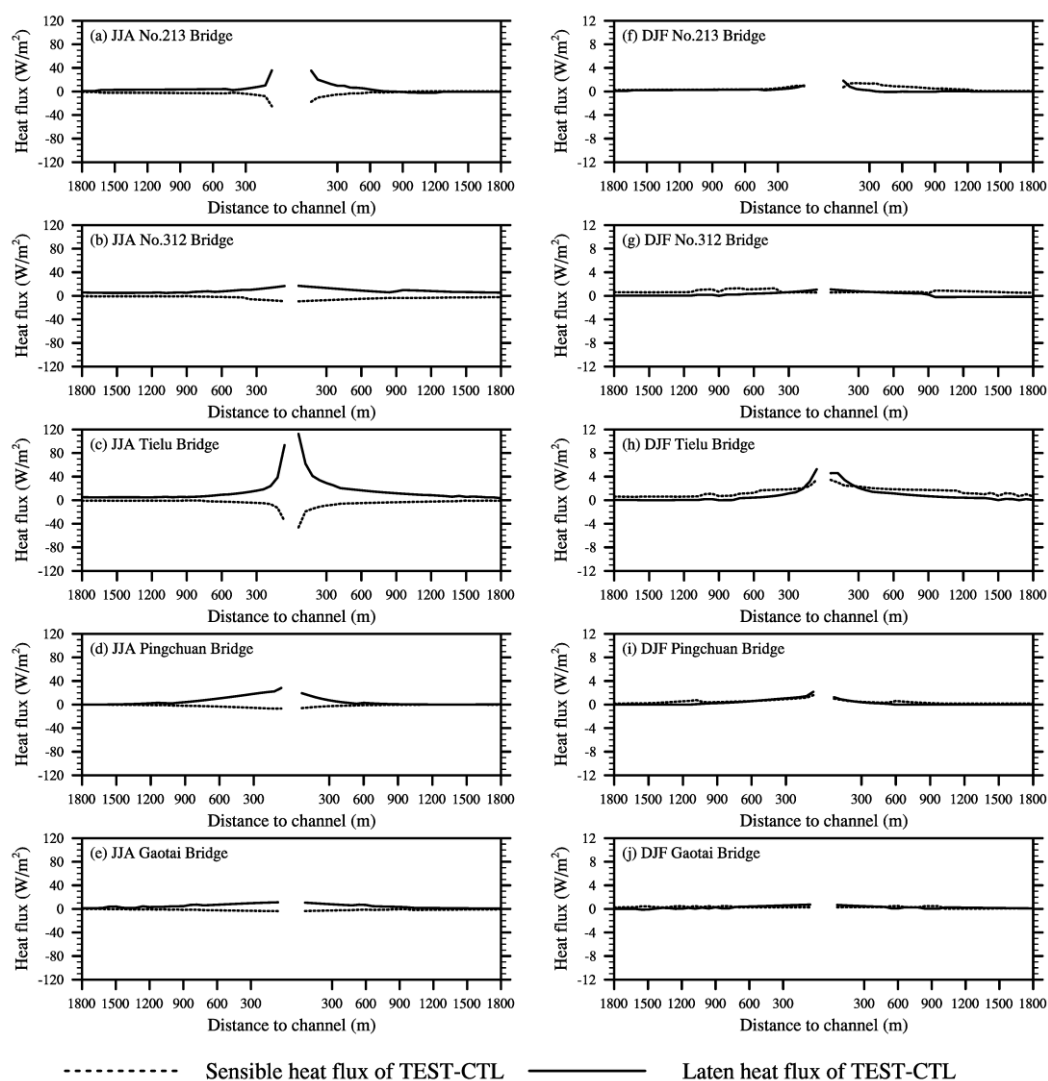


**Figure 16** Differences of (a–e) sensible and (f–j) latent heat fluxes predicted by TEST and CTL simulations along the five sections at (a and f) 213 Bridge, (b and g) 312 Bridge, (c and h) Tielu Bridge, (d and i) Pingchuan Bridge and (e and j) Gaotai Bridge. The discontinuous parts of the curves represent the river areas.